Applied Physics Letters ACCEPTED MANUSCRIPT
This is the author's peer reviewed, accepted manuscript. However, the online version of record will be different from this version once it has been copyedited and typeset.
PLEASE CITE THIS ARTICLE AS DOI: 10.1063/5.0167430
AIP Publishing

Influence of Trap-Assisted and Intrinsic Auger-Meitner Recombination on Efficiency Droop in Green InGaN/GaN LEDs

Xuefeng Li[1*], Elizabeth DeJong[1], Rob Armitage[2], Andrew M. Armstrong[3], and Daniel Feezell[1]

1Center for High Technology Materials (CHTM), University of New Mexico, Albuquerque, NM 87106, USA
2Lumileds LLC, San Jose, CA 95131, USA
3Sandia National Laboratories, Albuquerque, NM 87123, USA

We study the impact of deep-level defects on trap-assisted Auger-Meitner recombination in *c*-plane InGaN/GaN LEDs using a small-signal electroluminescence (SSEL) method and deep-level optical spectroscopy (DLOS). Carrier dynamics information, including carrier lifetime, recombination rate, and carrier density, are obtained from SSEL, while DLOS is used to obtain the deep-level defect density. Through fitting the nonradiative recombination rates of wafers with different deep-level defect densities, we obtain the Shockley-Read-Hall (SRH) and trap-assisted Auger-Meitner recombination (TAAR) coefficients. We show that defect-related nonradiative recombination, including both SRH and TAAR, accounts for a relatively small fraction of the total nonradiative recombination, which is dominated by intrinsic Auger-Meitner recombination. The interplay between carrier localization and Coulomb enhancement has a different impact on radiative and intrinsic Auger-Meitner recombination. Evidence is presented that the imbalance between the change of radiative and intrinsic Auger-Meitner recombination is the primary cause of the efficiency droop at high carrier densities in the samples studied.

[*]**Electronic mail:** xuefengli@unm.edu

Applied Physics Letters ACCEPTED MANUSCRIPT
AIP Publishing
This is the author's peer reviewed, accepted manuscript. However, the online version of record will be different from this version once it has been copyedited and typeset.
PLEASE CITE THIS ARTICLE AS DOI: 10.1063/5.0167430

Deep-level defects are known to negatively affect the efficiency of light-emitting diodes (LEDs) [1,2]. Deep-level defects contribute not only to Shockley–Read–Hall (SRH) recombination, but also to trap-assisted Auger-Meitner recombination (TAAR). The relationship between density of deep-level defects and the TAAR processes has been predicted theoretically [3,4] and observed experimentally [5,6] to a limited degree. However, some details about TAAR are still under debate, including its magnitude relative to SRH and intrinsic Auger-Meitner (IA) recombination [6,7,8], its dependence on carrier density (e.g., $\propto n^2$ or n^3) [6,7,8,9], and its role in the green gap. Of particular interest is the role of TAAR in LEDs grown with state-of-the-art growth conditions since TAAR is typically assumed to be linearly dependent on defect density, directly tying the magnitude of TAAR to the quality of the sample [7,8]. Previous studies have examined TAAR using time-resolved photoluminescence [6,8] and optical differential lifetime measurements [7], which do not capture electrical injection and carrier transport effects. Additionally, separate quantification of the deep-level defect densities was not performed in these studies. To determine whether nonradiative recombination associated with deep-level defects is limiting the radiative efficiency in state-of-the-art green InGaN/GaN LEDs, more research is needed to correlate the deep-level defect density to the relative magnitudes of the various nonradiative recombination mechanisms, which is critical to further improvement of the radiative efficiency of green InGaN/GaN LEDs.

In this work, we report a quantitative study of TAAR in *c*-plane green LEDs grown by metal-organic chemical vapor deposition (MOCVD) using state-of-the-art growth conditions. We investigate a series of three wafers (~ 530 nm) with identical active regions (3X, 3-nm-thick quantum wells with indium composition of 19%) but different deep-level defect densities ($4.5 \times 10^{14}\ cm^{-3} < N_t < 1.5 \times 10^{15}\ cm^{-3}$). Details about the defect densities are shown in Table 1. The barriers are GaN and are 18 nm thick. We use small-signal electroluminescence (SSEL) [10,11] and deep-level optical spectroscopy (DLOS) and lighted capacitance-voltage (LCV) [12] to study the carrier dynamics and density of deep-level defects in the samples, respectively. We investigate the relationship between the density of deep-level defects and the corresponding radiative and nonradiative recombination rates at a given *n* and show the respective roles of these mechanisms on the radiative efficiency.

SSEL is used to determine the carrier lifetime, which is used in conjunction with the internal quantum efficiency (IQE) to decouple the radiative and nonradiative recombination rates. The details of the SSEL setup and measurement

AIP Publishing
Applied Physics Letters ACCEPTED MANUSCRIPT
This is the author's peer reviewed, accepted manuscript. However, the online version of record will be different from this version once it has been copyedited and typeset.
PLEASE CITE THIS ARTICLE AS DOI: 10.1063/5.0167430

procedure can be found in Ref. 13. Following the analysis in Ref. 13, multiple transport and recombination parameters can be extracted using this method. As shown in Figure 1(a), the injection efficiencies for the growth quality series are nearly identical. The internal quantum efficiency (IQE) shown in Figure 1(b) was obtained from Lumileds by measuring the external quantum efficiency (EQE) of LEDs with known extraction efficiency. The IQE varies by approximately 10% points between each growth quality at low current density (*J*) but is comparable at high current density. The radiative efficiency was obtained from the IQE and the injection efficiency using $\eta_{IQE} = \eta_{inj} * \eta_r$, and is shown in Figure 1(c). All three samples display a similar radiative efficiency at high carrier density, a behavior that is not suggestive of an n^3 process. Furthermore, TAAR was theoretically shown to have an n^2 dependency [4,9] due to the fact that, although it's a three-carrier process, only two free carriers are involved, with the third carrier located at the deep-level defects [3].

Growth Quality	Good	Middle	Bad
N_t [$\times 10^{15}\ cm^{-3}$]	0.45	0.78	1.50
A [$\times 10^{6}\ s^{-1}$]	2.15	3.73	7.18
D [$\times 10^{-13}\ cm^3 s^{-1}$]	0.58	1.00	1.92

Table 1. Deep-level defect density in the growth quality series measured using DLOS and corresponding *A* and *D* parameters from fittings.

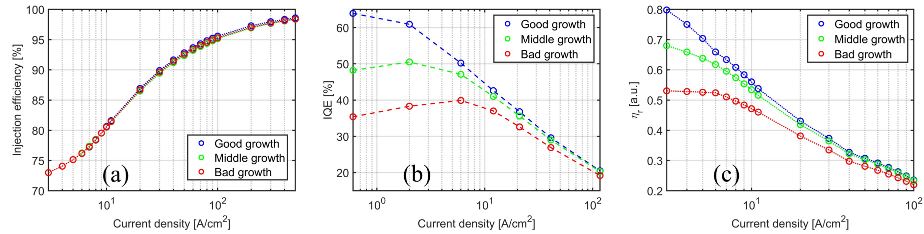

FIG. 1. (a) Injection efficiency, (b) IQE, and (c) Radiative efficiency vs. current density (*J*) for good, middle, and bad growth.

In SSEL, the total recombination lifetime can be calculated from the integration of the differential recombination lifetime, which is directly acquired from the simultaneous fitting of the impedance and modulation responses of the LED. By utilizing the recombination lifetime and the radiative efficiency obtained from the previous section, the radiative and nonradiative recombination lifetimes are readily separated from the total recombination lifetime [14]. The total recombination lifetime in higher quality growth is found to be longer than that in lower quality growth at

AIP Publishing Applied Physics Letters ACCEPTED MANUSCRIPT
This is the author's peer reviewed, accepted manuscript. However, the online version of record will be different from this version once it has been copyedited and typeset.
PLEASE CITE THIS ARTICLE AS DOI: 10.1063/5.0167430

low and moderate current densities, as shown in Figure 2(a). This is attributed to higher quality samples having longer nonradiative recombination lifetimes, as illustrated in Figure 2(b). The radiative recombination lifetimes are similar in all three samples across the full range of current densities. In Figure 2(c), the bad growth has a lower n at a given J due to the higher nonradiative recombination rate caused by the increased density of deep-level defects.

The radiative and nonradiative rates can be calculated from the carrier density in the active region and the corresponding radiative and nonradiative lifetimes [14]. Since the IQEs vary by around 10% at low J but are similar at high J, we observed a significant difference in nonradiative recombination rates at low n and a relatively small difference in nonradiative recombination rates at high n, as shown in Figure 2(d). On the other hand, the radiative recombination rates for different growth qualities at a given n are identical, as expected from samples with the same active region design. At steady state, carriers injected into the QWs recombine via multiple recombination mechanisms: $\frac{J}{qd} = An + B(n)n^2 + C(n)n^3 + Dn^2$. Here, A, $B(n)$, $C(n)$, and D are associated with SRH, radiative, IA, and TAAR, respectively. Here, q is elementary charge and d is total QW thickness. While the total recombination rates ($\frac{J}{qd}$) remain constant across the growth quality series, the deep-level defect-related nonradiative recombination coefficients (A and D) are higher for lower quality growths at a given J. Thus, the carrier density is inherently lower for the lower quality growths at a given J, as shown in Figure 2(c). A similar analysis can be found in Ref. 13.

DLOS/LCV was used to measure the density of deep-level defects (N_t) (alternatively referred to as non-radiative recombination centers (NRCs)) to understand variations in A across LEDs. DLOS is a photocapacitance technique that measures the optical absorption spectrum of a deep level from the time-dependence of change in space-charge in a depletion region when the defect changes charge state upon photoemission. A 150 W Xe lamp filtered through a $1/4$ meter monochromator provided monochromatic optical excitation from near-infra-red to ultra-violet. DLOS measurements were performed at an electrical bias that restricted the depletion region and hence DLOS sensitivity to the multi-quantum well (MQW) region, as confirmed by C-V profiling. A deep level with an approximate energy of 1.7 eV below the conduction band minimum (E_c) was observed. Its energy was determined by fitting its optical absorption line-shape to a theoretical model accounting for electron-phonon coupling [15]. The E_c – 1.7 eV deep level was attributed to the QWs because subsequent investigations found its optical absorption line-shape varied strongly with QW InN mole fraction. The defect concentration for the E_c – 1.7 eV deep state was measured using LCV. LCV

ACCEPTED MANUSCRIPT
Applied Physics Letters
AIP Publishing
This is the author's peer reviewed, accepted manuscript. However, the online version of record will be different from this version once it has been copyedited and typeset.
PLEASE CITE THIS ARTICLE AS DOI: 10.1063/5.0167430

compares *C-V* measurements taken in the dark with the deep level occupied and under 2.1 eV illumination with the deep level optically depopulated. The Poisson equation relates the increase in space-charge density, i.e., N_t, in the depletion region due to photoemission from the deep level to the change in voltage (ΔV) required to maintain the junction depletion depth at the edge of the MQW region. In this analysis, it was assumed that the E_c – 1.7 eV deep level occupancy changed from fully occupied in the dark to empty under illumination and that the defect concentration was the same in each QW.

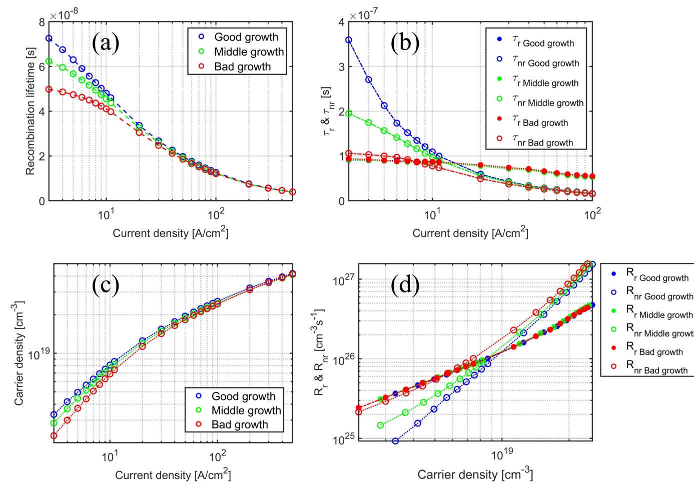

FIG. 2. (a) Total recombination lifetime vs. current density (*J*), (b) Radiative and non-radiative lifetimes vs. current density (*J*), (c) Carrier density (*n*) vs. current density (*J*), and (d) Radiative and non-radiative recombination rates vs. carrier density (*n*) for good, middle, and bad growth.

The recombination rate and deep-level defect information are acquired using SSEL and DLOS, respectively and independently. We extract the relationship between the density of deep-level defects and their corresponding nonradiative recombination rates at a given *n*. The total nonradiative recombination rate is decomposed into three components: SRH, IA, and TAAR. This can be expressed as:

$$R_{nr} = R_{SRH} + R_{IA} + R_{TAAR} = An + C(n)n^3 + Dn^2 = C(n)n^3 + A(n + k_D n^2) \quad (1)$$

Here, the term Dn^2 represents the TAAR rate, as described in Ref 6, Ref 8, and Ref 9. The ratio between D and A is denoted by k_D. The SRH and TAAR rates are proportional to N_t, while IA is not and should be the same for all three samples. Therefore, the A and D parameters can be expressed as: $A = \alpha N_t$ and $D = \alpha k_D N_t$. Thus, the difference in

Applied Physics Letters ACCEPTED MANUSCRIPT
AIP Publishing
This is the author's peer reviewed, accepted manuscript. However, the online version of record will be different from this version once it has been copyedited and typeset.
PLEASE CITE THIS ARTICLE AS DOI: 10.1063/5.0167430

nonradiative recombination rates (ΔR_{nr}) between samples of different growth qualities results only from changes in SRH and TAAR and can be expressed as:

$$\Delta R_{nr} = R_{nr2} - R_{nr1} = \Delta An + \Delta Dn^2 = \alpha \Delta N_t (n + k_D n^2) \quad (2)$$

where α is related to the capture cross section associated with deep-level defect density, ΔN_t is the difference in deep-level defect densities, and ΔA is the difference in the *A* coefficients between different growth qualities.

To compare the ΔR_{nr} between the bad and good growth samples, and the bad and middle growth samples, we scale them to a ΔN_t of $1 \times 10^{15}\ cm^{-3}$. In Figure 3(a), we plot the normalized ΔR_{nr} vs. *n* and observe that the two sets of data are almost overlapped at low *n,* and remain close at higher *n*. This confirms the linear relationship between the SRH and TAAR recombination rates and N_t, as ΔR_{nr} is proportional to ΔN_t. Here, normalized ΔR_{nr} and ΔN_t were acquired from SSEL and DLOS, respectively.

Next, we investigate the relationship between the normalized ΔR_{nr} and n to obtain the values for the ΔA and ΔD by fitting equation 2. The ΔA and ΔD parameters are acquired from the differences between the bad and good growth samples, and the bad and middle growth samples. The ΔA and ΔD parameters are found to be $\Delta A = 4.50 \times 10^6 s^{-1}$ and $\Delta D = 1.89 \times 10^{-13} cm^3 s^{-1}$ using data from bad to good samples, and $\Delta A = 5.07 \times 10^6 s^{-1}$ and $\Delta D = 6.73 \times 10^{-14} cm^3 s^{-1}$ using data from bad to middle samples. We use the average of these parameters, $\Delta A_{avg} = 4.79 \times 10^6 s^{-1}$ and $\Delta D_{avg} = 1.28 \times 10^{-13} cm^3 s^{-1}$ for the subsequent calculations and scale the corresponding values using the ΔN_t and N_t for the three wafers using: $A = \frac{\Delta A_{avg}}{\Delta N_t} \times N_t$ and $D = \frac{\Delta D_{avg}}{\Delta N_t} \times N_t$. We note that small variations in the values of ΔA_{avg} and ΔD_{avg} do not strongly affect the following analysis and conclusions due to the small relative roles of SRH and TAAR on the total nonradiative recombination rates. The values of *A* and *D* parameters in the growth quality series are shown in Table 1. The coefficient $k_D = 2.68 \times 10^{-20} cm^3$, while the TAAR recombination coefficients *D* for these green LEDs are on the order of $\sim 1 \times 10^{-13} cm^3 s^{-1}$, which is comparable to that reported for violet LEDs (also using an n^2 model), indicating the weak dependence of TAAR on bandgap [8]. Although the n^2 dependency of TAAR is commonly used in experiment studies [6,8] and supported by theoretical research [3,4,9], we still cannot completely exclude the possibility of an n^3 dependency in this paper. The fitting results for an n^3 dependency are available in supplementary materials and the different *n* dependency won't change the conclusions.

Applied Physics Letters ACCEPTED MANUSCRIPT
This is the author's peer reviewed, accepted manuscript. However, the online version of record will be different from this version once it has been copyedited and typeset.
PLEASE CITE THIS ARTICLE AS DOI: 10.1063/5.0167430
AIP Publishing

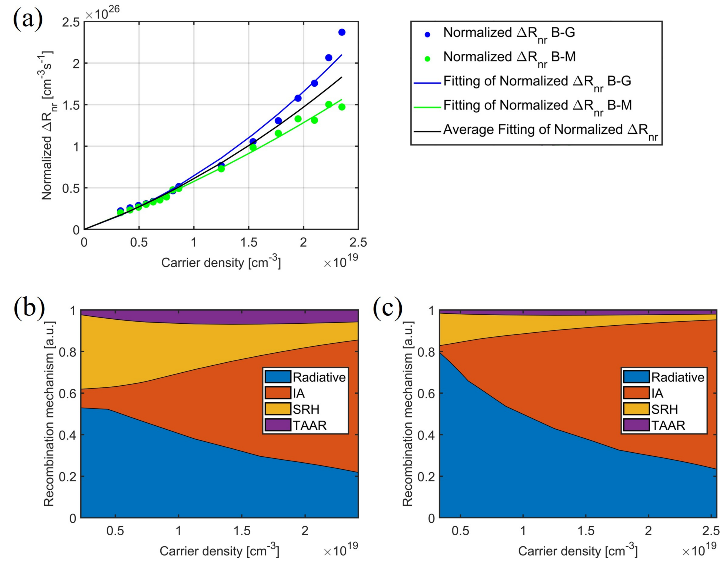

FIG. 3. (a) Normalized ΔR_{nr} data and fitting vs. carrier density (*n*) for bad to good, and bad to middle growth. Solid dots are experimental data, solid lines are fitting of normalized ΔR_{nr}. (b)&(c) The percentage of every recombination mechanism vs. carrier density (*n*) in bad and good growth wafer.

With the *A* and *D* parameters obtained the IA recombination can be obtained by subtracting the SRH and TAAR from the total nonradiative recombination rate. Here, the intrinsic Auger-Meitner recombination can be expressed as:

$$R_{IA} = R_{nr} - An - Dn^2 \quad (3)$$

To better understand the role of each recombination mechanism at various carrier densities, we calculated the proportion of each mechanism to the total recombination rate in the bad and good growth wafers. The relative values of the various recombination mechanisms are illustrated in Figure 3(b) and 3(c), respectively. The percentage of radiative recombination is equivalent to the radiative efficiency shown in Figure 1(c) but with a carrier density x-axis. The significance of IA increases at higher carrier densities, while the importance of SRH declines. Furthermore, the SRH recombination is of the same order as TAAR and should not be disregarded when considering efficiency decline, even at high carrier densities. The TAAR percentage remains below 7% and 3% of the total recombination throughout the range of carrier densities in bad and good growth, as shown in Figure 3(b) and 3(c), respectively. In the samples

AIP Publishing Applied Physics Letters ACCEPTED MANUSCRIPT
This is the author's peer reviewed, accepted manuscript. However, the online version of record will be different from this version once it has been copyedited and typeset.
PLEASE CITE THIS ARTICLE AS DOI: 10.1063/5.0167430

studied, intrinsic Auger-Meitner recombination still dominates the nonradiative recombination and TAAR is not found to be a significant contributor to droop or the green gap.

With the radiative recombination rate (R_r), the IA recombination rate (R_{IA}), and the carrier density (n) known, the coefficients $B(n) = {R_r}/{n^2}$ and $C(n) = {R_{IA}}/{n^3}$, associated with bimolecular and intrinsic Auger-Meitner recombination, can be calculated and are shown in Figure 4(a) and 4(b) [16]. Figure 4(a) shows the $B(n)$ coefficients, which are essentially the same for all three samples. The fact that all the $B(n)$ coefficients are the same confirming the accuracy of using SSEL to measure the carrier dynamics since the three samples all have different IQEs and lifetimes. In thin quantum wells, $B(n)$ and $C(n)$ are influenced by several mechanisms, including the quantum-confined Stark effect (QCSE) [17-20], phase space filling effect (PSF) [16], carrier localization [7,21-25], and Coulomb enhancement [23]. QCSE and PSF have a similar effect on both radiative and nonradiative recombination rates [16,26]. Carrier localization increases both radiative and intrinsic Auger-Meitner recombination rates but has more of an impact on intrinsic Auger-Meitner recombination [22]. However, the strong $B(n)$ enhancement frequently observed in both electrical injection [13,27] and optically pumped LEDs [23] with thin QWs at low n cannot be explained simply by carrier localization. Conversely, Coulomb enhancement is a mechanism that can significantly increase the radiative recombination rate in thin quantum wells at low n, and this effect is gradually screened until it reaches the free-carrier limit at high n [23]. Both carrier localization and Coulomb enhancement increase $B(n)$ and $C(n)$ at low n. However, in Figure 4(b), $C(n)$ remains relatively steady with carrier density, suggesting relatively lower Coulomb enhancement compared to $B(n)$. As demonstrated in the previous section, the impact of defect-associated mechanisms (i.e., $An + Dn^2$) is limited and the radiative efficiency is mostly determined by radiative and intrinsic Auger-Meitner recombination at high n. Considering the all mechanisms in III-nitride LEDs discussed above, the radiative efficiency at high n can be expressed as:

$$\eta_r = \frac{1}{1 + \frac{C(n) * n^3}{B(n) * n^2}} = \frac{1}{1 + k * n * g(n)} \tag{4}$$

where k is a constant value related to the intrinsic properties of InGaN/GaN and $g(n)$ is related to the effect of carrier localization and Coulomb enhancement on $C(n)$ and $B(n)$ terms. The second equality assumes QCSE and PSF cancel

ACCEPTED MANUSCRIPT
Applied Physics Letters
AIP Publishing
This is the author's peer reviewed, accepted manuscript. However, the online version of record will be different from this version once it has been copyedited and typeset.
PLEASE CITE THIS ARTICLE AS DOI: 10.1063/5.0167430

in the ratio $C(n)/B(n)$ [16,26], leaving a constant k and $g(n)$, which depends only on carrier localization and Coulomb enhancement.

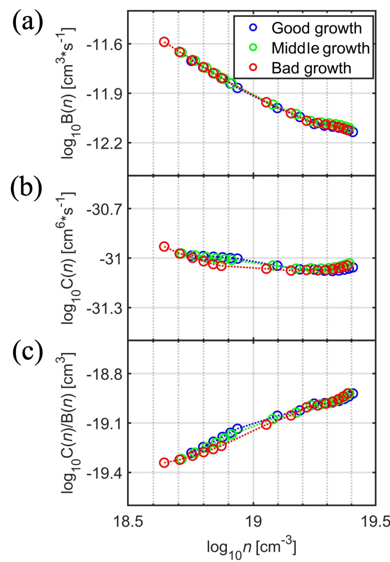

FIG. 4. (a)-(c) $B(n)$ & $C(n)$ coefficients and the ratios of $C(n)/B(n)$ vs. carrier density (*n*) for good, middle, and bad growth.

For a given sample, the radiative efficiency in Equation (4) is driven by two factors: the carrier density (*n*) and the ratio $C(n)/B(n)$. The effect of the carrier density on equation (4) for different samples is minor, as the carrier densities are similar for middle to high current density for different growth qualities, as shown in Figure 2(c). At low *J*, the IQE of green InGaN/GaN LEDs is above 60%, but the value drops to only 30% at 40 A/cm^2, even for the highest growth quality sample. The present work rules out TAAR as an explanation for the poor high-*J* performance of green LEDs with state-of-the-art epitaxy. Thus, the rapid decrease in IQE with *J* can only be explained from the ratio $C(n)/B(n)$. Figure 4(c) shows the ratio of $C(n)/B(n)$, which increases as the carrier density rises, indicating a decrease of the radiative efficiency. The decrease in radiative efficiency is partially due to IA recombination but is also associated with reduced carrier localization and Coulomb enhancement of $B(n)$ at higher n as carriers become more delocalized [23]. While $B(n)$ strongly increases at low n, $C(n)$ does not follow the same trend in the present samples, leading to

AIP Publishing Applied Physics Letters ACCEPTED MANUSCRIPT
This is the author's peer reviewed, accepted manuscript. However, the online version of record will be different from this version once it has been copyedited and typeset.
PLEASE CITE THIS ARTICLE AS DOI: 10.1063/5.0167430

enhanced radiative efficiency at low n. Thus, the apparent efficiency droop is a combination of IA recombination and reduction of Coulomb enhancement of the radiative rate. A lower carrier density at a given J is therefore beneficial to high radiative efficiency by reducing IA recombination and operating in a regime that leverages the disparity in Coulomb enhancement effects between $B(n)$ and $C(n)$.

In summary, we studied the impact of deep-level defects on nonradiative recombination rates in state-of-the-art growth green InGaN/GaN LEDs using SSEL and DLOS. By analyzing the nonradiative recombination rates in wafers of varying growth quality, we obtained the coefficients for SRH and TAAR, and neither of the two mechanisms was found to significantly contribute to the efficiency droop observed in the green InGaN/GaN LEDs studied. Instead, intrinsic Auger-Meitner recombination was found to be the primary mechanism for nonradiative recombination. The efficiency droop can be attributed to the imbalance between radiative and intrinsic Auger-Meitner recombination due to carrier localization and Coulomb enhancement in the LEDs studied. Thus, maintaining a low carrier density in thin QWs is advantageous for avoiding strong intrinsic Auger-Meitner recombination and utilizing the interplay of carrier localization and Coulomb enhancement on the radiative process.

See the supplementary material for the fitting of normalized ΔR_{nr} data using an n^3 dependency for TAAR.

This work was supported by the Department of Energy under Award No. DE-EE0009163. Sandia National Laboratories is a multimission laboratory managed and operated by National Technology & Engineering Solutions of Sandia, LLC, a wholly owned subsidiary of Honeywell International Inc., for the U.S. Department of Energy's National Nuclear Security Administration under contract DE-NA0003525. This paper describes objective technical results and analysis. Any subjective views or opinions that might be expressed in the paper do not necessarily represent the views of the U.S. Department of Energy or the United States Government.

[1] A.M. Armstrong, M.H. Crawford, and D.D. Koleske, Applied Physics Express 7, 032101 (2014).

AIP Publishing
Applied Physics Letters ACCEPTED MANUSCRIPT
This is the author's peer reviewed, accepted manuscript. However, the online version of record will be different from this version once it has been copyedited and typeset.
PLEASE CITE THIS ARTICLE AS DOI: 10.1063/5.0167430

[2] S. Hammersley, M.J. Kappers, F.C.-P. Massabuau, S.-L. Sahonta, P. Dawson, R.A. Oliver, and C.J. Humphreys, Appl. Phys. Lett. 107, 132106 (2015).
[3] L. Bess, Physical Review 111, 129 (1958).
[4] P. T. Landsberg, C. Rhys-Roberts, and P. Lal, Proc. Phys. Soc. 84, 915 (1964).
[5] D.J. Myers, A.C. Espenlaub, K. Gelzinyte, E.C. Young, L. Martinelli, J. Peretti, C. Weisbuch, and J.S. Speck, Appl. Phys. Lett. 116, 091102 (2020).
[6] A.C. Espenlaub, D.J. Myers, E.C. Young, S. Marcinkevičius, C. Weisbuch, and J.S. Speck, Journal of Applied Physics 126, 184502 (2019).
[7] A. David, N.G. Young, C.A. Hurni, and M.D. Craven, Phys. Rev. Applied. 11, 031001(2019).
[8] W. Liu, C. Haller, Y. Chen, T. Weatherley, J.-F. Carlin, G. Jacopin, R. Butté, and N. Grandjean, Appl. Phys. Lett. 116, 222106 (2020).
[9] F. Zhao, M. E. Turiansky, A. Alkauskas, and C. G. Van de Walle, Phys. Rev. Lett. 131, (2023).
[10] A. David, C.A. Hurni, N.G. Young, and M.D. Craven, Appl. Phys. Lett. 109, 033504 (2016).
[11] A. Rashidi, M. Nami, M. Monavarian, A. Aragon, K. DaVico, F. Ayoub, S. Mishkat-Ul-Masabih, A. Rishinaramangalam, and D. Feezell, J. Appl. Phys. 122, 035706 (2017).
[12] A. Armstrong, T.A. Henry, D.D. Koleske, M.H. Crawford, and S.R. Lee, Optics Express 20, (2012).
[13] X. Li, N. Pant, E. DeJong, A.T. Elshafiey, R. Armitage, E. Kioupakis, and D. Feezell, Appl. Phys. Lett. 122, 212108 (2023).
[14] A. Rashidi, M. Monavarian, A. Aragon, and D. Feezell, Sci. Rep. 9, 19921 (2019).
[15] R. Pässler, Journal of Applied Physics 96(1), 715 (2004).
[16] A. David and M.J. Grundmann, Appl. Phys. Lett. 96, 103504 (2010).
[17] A. David and M.J. Grundmann, Appl. Phys. Lett. 97, 033501 (2010).
[18] E. Kioupakis, Q. Yan, and C.G. Van de Walle, Appl. Phys. Lett. 101, 231107 (2012).
[19] T. Takeuchi, S. Sota, M. Katsuragawa, M. Komori, H. Takeuchi, H. Amano, and I. Akasaki, Jpn. J. Appl. Phys., Part 2 36, L382 (1997).
[20] J. Bai, T. Wang, and S. Sakai, J. Appl. Phys. 88, 4729 (2000).
[21] M. Auf der Maur, A. Pecchia, G. Penazzi, W. Rodrigues, and A. Di Carlo, Phys. Rev. Lett. 116, (2016).
[22] C.M. Jones, C.-H. Teng, Q. Yan, P.-C. Ku, and E. Kioupakis, Appl. Phys. Lett. 111, 113501 (2017).
[23] A. David, N.G. Young, and M.D. Craven, Physical Review Applied 12, 044059 (2019).
[24] D.S.P. Tanner, P. Dawson, M.J. Kappers, R. Oliver and S. Schulz. Phys. Rev. Applied. 13, 044068 (2020).
[25] J. Hader, J. V. Moloney, and S. W. Koch, Appl. Phys. Lett. 96, 221106 (2010).
[26] A. David, N.G. Young, C. Lund, and M.D. Craven, Appl. Phys. Lett. 115, 193502 (2019).
[27] Y.C. Chow, C. Lynsky, S. Nakamura, S.P. DenBaars, C. Weisbuch, and J.S. Speck, Appl. Phys. Lett. 121, 181102 (2022).